LPL-positive endothelial cells control T cell homing in liver metastasis

Xiaowen Zhang, Miki Kamiyama, Margaret Tulessin, Lorna Rinck, Jan-Philipp Mallm, Michael Kilian, Dennis A. Agardy, Mathias Heikenwälder, Michael Platten, Carolin Mogler, Mahak Singhal*, Hellmut G. Augustin*

Supplementary Data File

Figures S1-17

Supplementary Figure S1

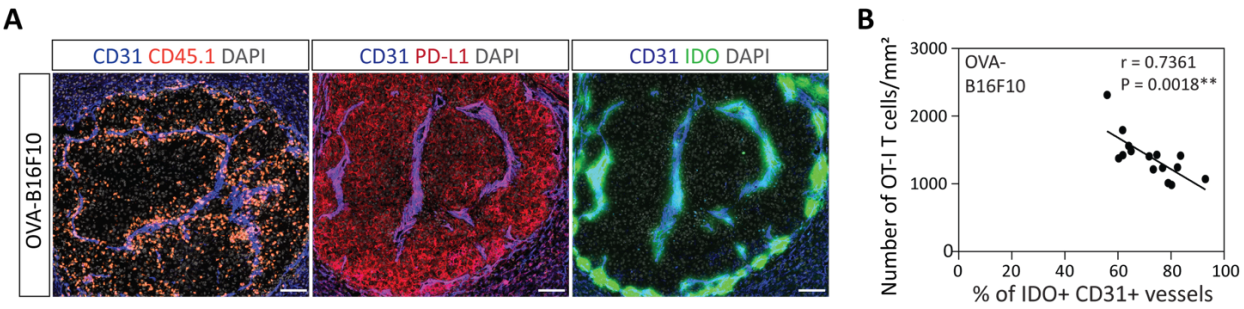

Supplementary Figure S1. Endothelial cells regulate effector T cell homing in OVA-B16F10 liver metastases.

(A) Representative images of CD31, CD45.1, PD-L1, IDO and DAPI stainings on liver metastatic tumors of OVA-B16F10 collected at 4 days after ACT. Scale bar: 100 μm.

(B) Pearson's correlation between the number of tumor-infiltrated OT-I T cells and the percentage of IDO-expressing CD31+ blood vessels. Tumor nodules were collected and analyzed from N = 3-5 mice.

Supplementary Figure S2

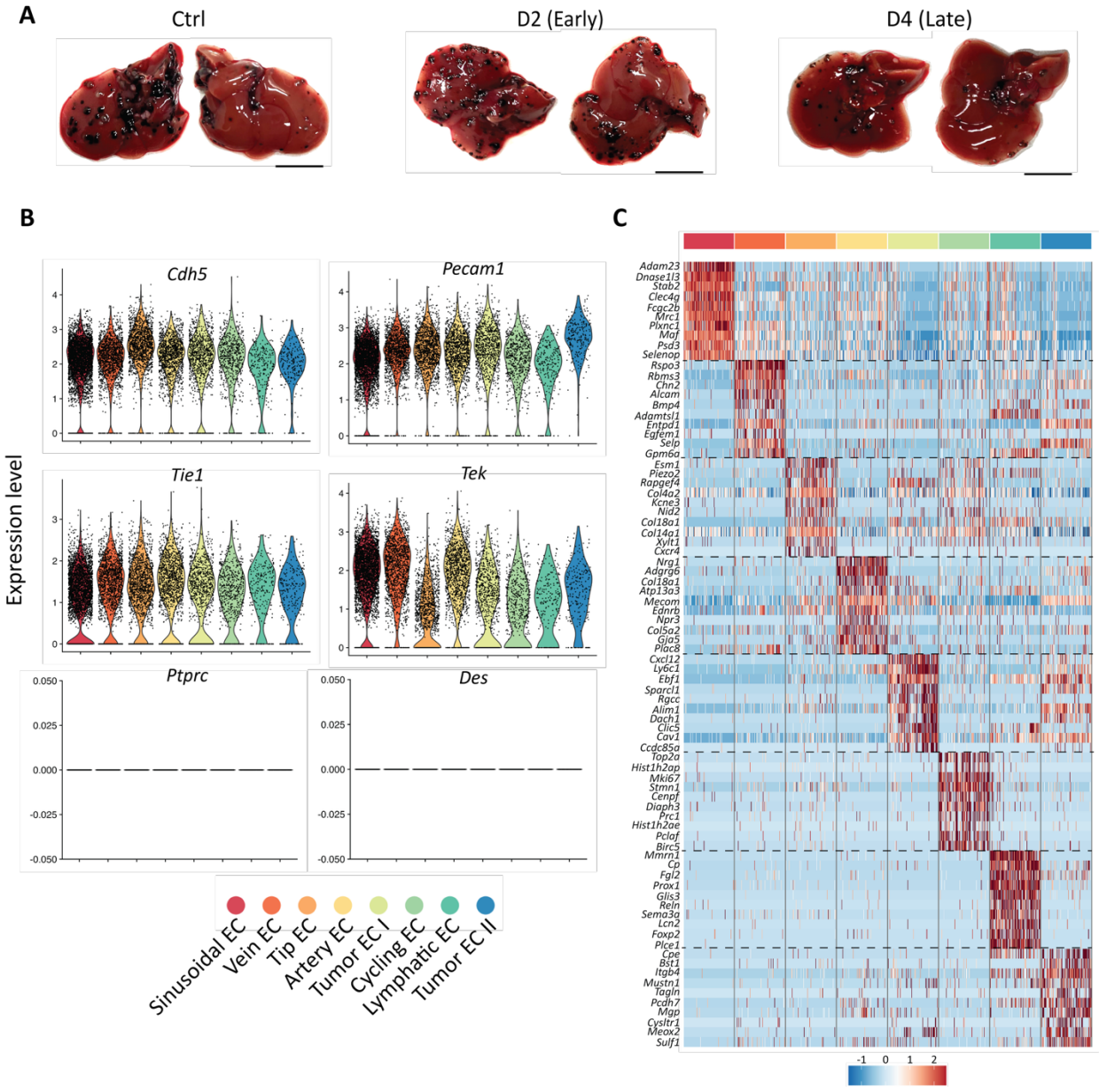

Supplementary Figure S2. Quality control of scRNAseq data of all analyzed ECs.

(A) Representative front and back images of OVA-B16F10 tumor-bearing livers collected at different time points after ACT of OT-I T cells or control PBS. Scale bar: 1 cm.

(B) Violin plots showing the expression of cell-type specific marker genes on each identified EC subpopulations**.**

(C) Heatmap on gene signature of different EC subsets based on top differential genes in each cluster.

Supplementary Figure S3

A

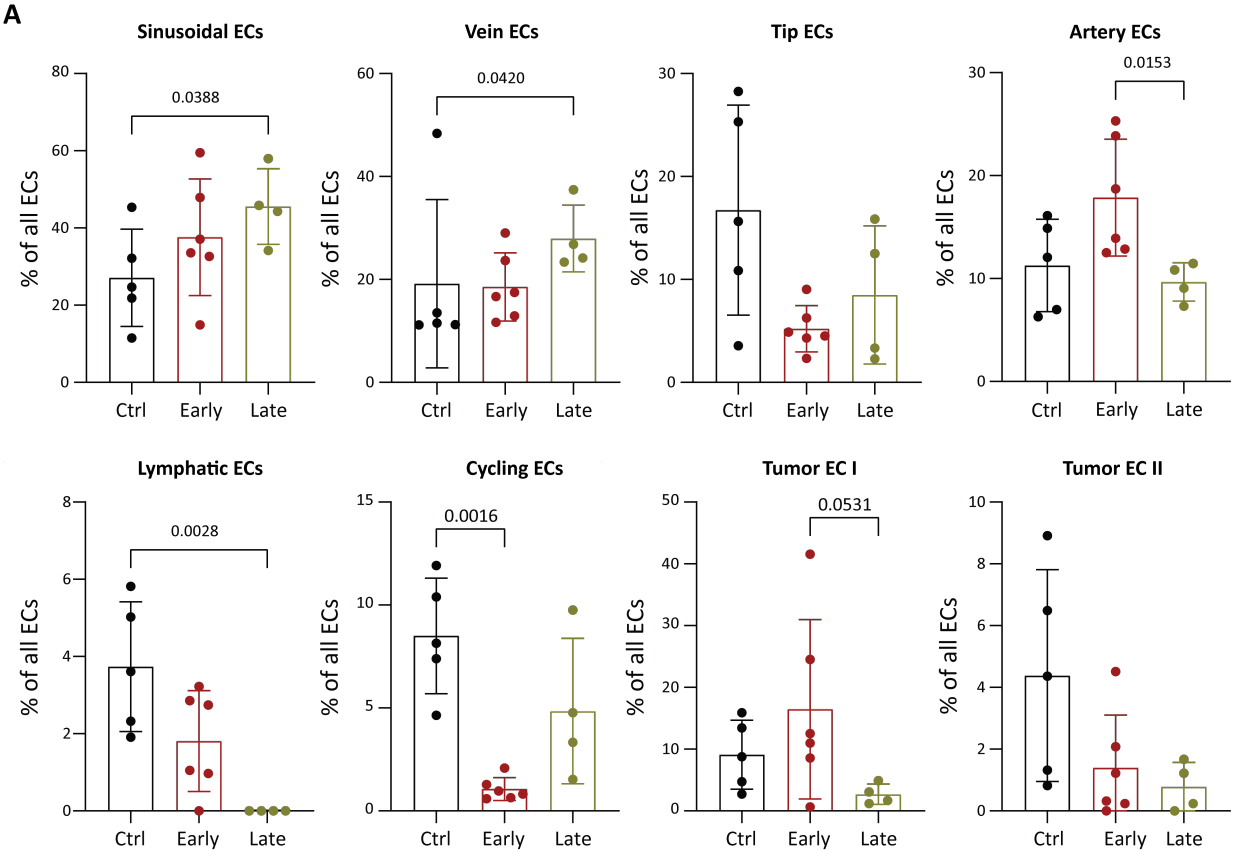

Supplementary Figure S3. Changes in the cluster composition of analyzed ECs following ACT.

(A) Quantitation of the fraction of each EC cluster from Ctrl-, Early- or Late-libraries. Data are presented as mean ± s.d. N = 4-6 mice per library. One-way ANOVA test. *P*-values without statistical significance are not shown in the figure.

Supplementary Figure S4

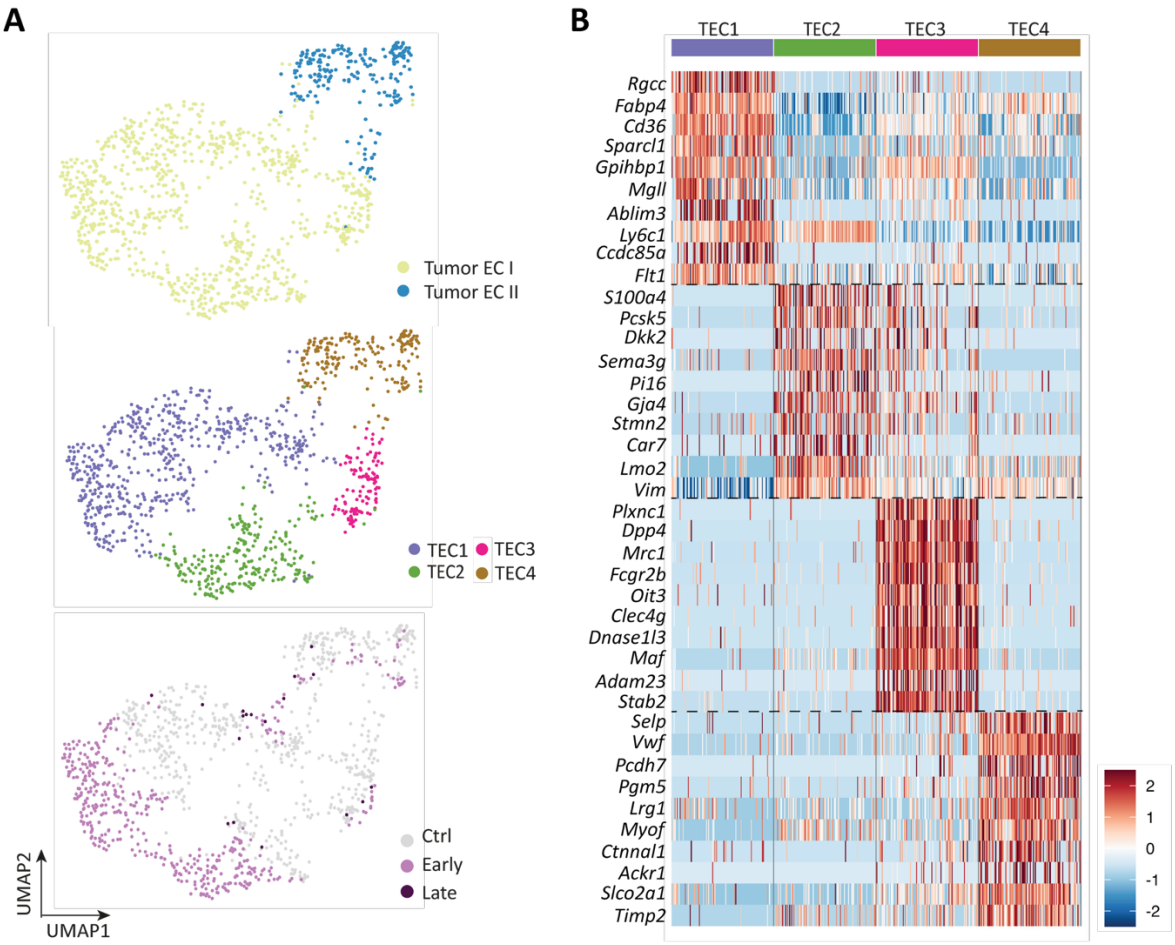

Supplementary Figure S4. Annotation of different tumor EC subsets.

(A) Top, UMAP visualization of tumor ECs (TECs) color-coded on the original Tumor EC I and Tumor EC II clusters from all analysed ECs. Middle, UMAP visualization of reclustered TECs into four color-coded subclusters – TEC1, TEC2, TEC3 and TEC4. Bottom, UMAP visualization of reclustered TECs color-coded on Ctrl-, Early- and Late- libraries.

(B) Heatmap of marker genes for each TEC subcluster.

Supplementary Figure S5

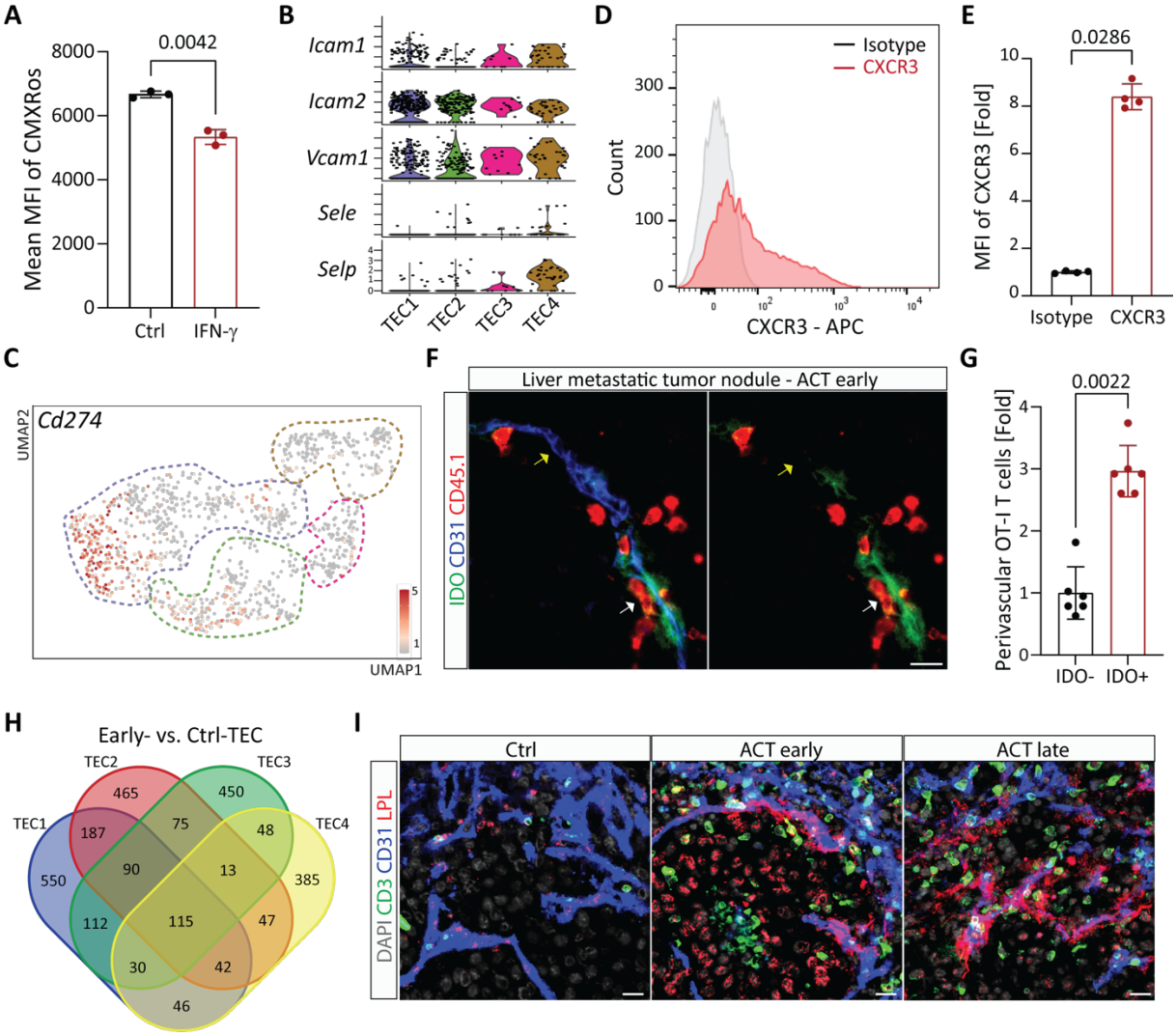

Supplementary Figure S5. scRNAseq-guided molecular characterization of TECs.

(A) Flow cytometric analysis of mitochondrial activity (CMXROS) in ECs treated with 100 ng/ml of IFN-γ or PBS as Ctrl. N = 3 independent experiments. Data are presented as mean ± s.d. Two-tailed student's T test.

(B) Violin plot showing the expression of adhesion molecule genes across different TEC subsets at Early timepoint.

(C) Feature plot showing *Cd274* expression across all TEC subsets.

(D,E) Cytometric analysis **(D)** and quantitation **(E)** of surface CXCR3 levels on activated OT-I T cells. N = 4 per group. Data are presented as mean ± s.d., normalized to isotype stained samples. Two-tailed Mann-Whitney U test.

(F) Representative IF images of IDO and CD45.1 staining on liver metastatic OVA-B16F10 tumors collected at the Early time point after ACT. Scale bar: 200 μm. Yellow and white arrows highlight IDO- and IDO+ perivascular niches in liver metastatic OVA-B16F10 tumors, respectively.

(G) Quantitation of OT-I T cells at IDO- and IDO+ perivascular niches in liver metastatic OVA-B16F10 tumors collected at the Early time point after ACT. Each dot represents average T cell numbers from one mouse liver sample. N= 5 mice. Data are presented as mean ± s.d., normalized to IDO- samples Two-tailed Mann-Whitney U test.

(H) Venn plot of the number of DEGs in each TEC subset between Early- and Ctrl-libraries.

(I) Representative images of LPL, CD3, CD31 and DAPI stainings on OVA-B16F10 liver metastatic tumors collected from Ctrl, Early, and Late time points after ACT. Scale bar: 10 μm.

Supplementary Figure S6

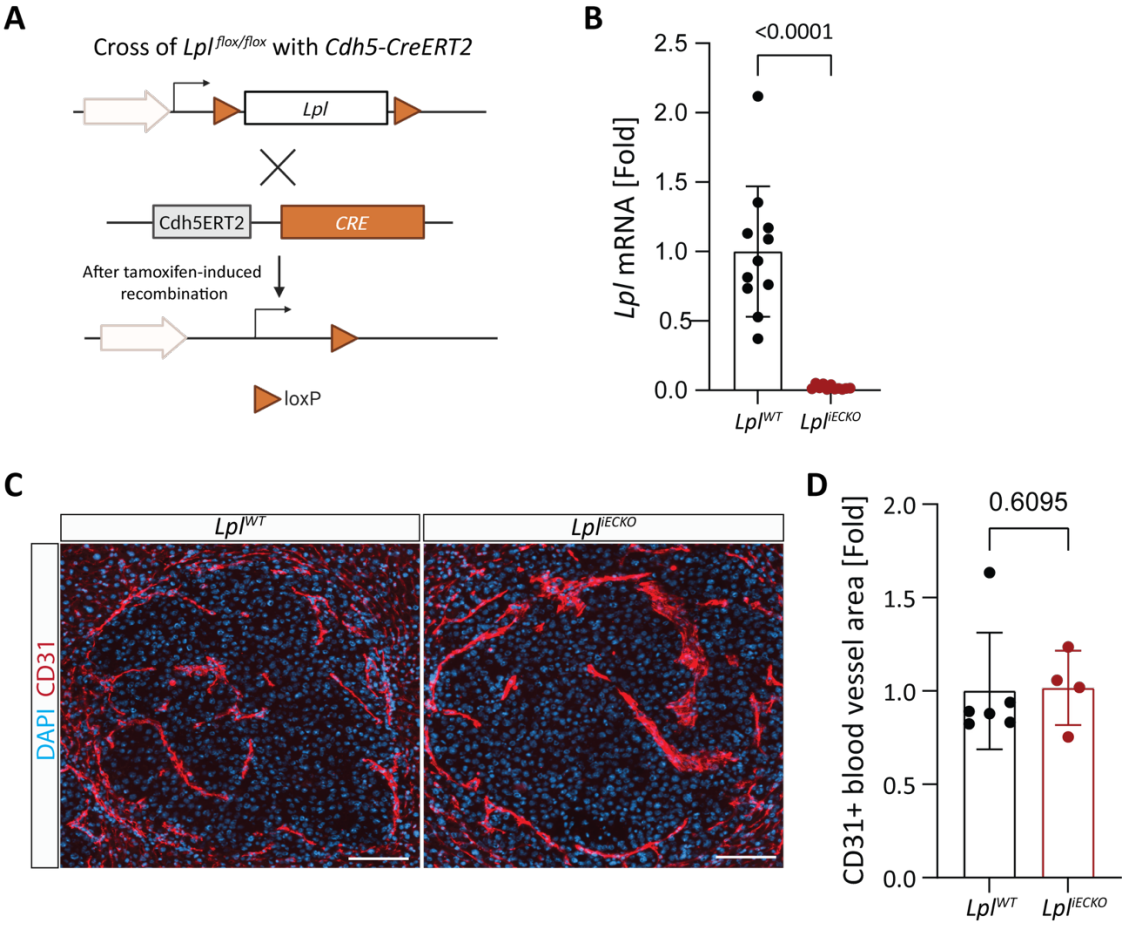

Supplementary Figure S6. Genetic deletion of *Lpl* in ECs and its influence on intratumoral vessels.

(A) Schematic diagram of tamoxifen-induced deletion of *Lpl* in ECs by crossing *Lpl*$^{flox/flox}$ with *Cdh5-CreERT2* mice.

(B) QPCR quantitation of *Lpl* expression in heart ECs from tamoxifen-treated *Lpl*^{WT} and *Lpl*^{iECKO} mice. N = 12-15 mice per group. Data are presented as mean ± s.d., normalized to *Lpl*^{WT} samples. Two-tailed Mann-Whitney U test.

(C) Representative images of CD31 stained liver OVA-B16F10 metastatic tumors. Scale bar: 100 μm.

(D) Quantitation of intratumoral blood vessel area in liver metastatic tumors from tamoxifen-treated *Lpl*^{WT} and *Lpl*^{iECKO} mice. N = 4-6 mice per group. Data are presented as mean ± s.d., normalized to *Lpl*^{WT} samples. Two-tailed Mann-Whitney U test.

Supplementary Figure S7

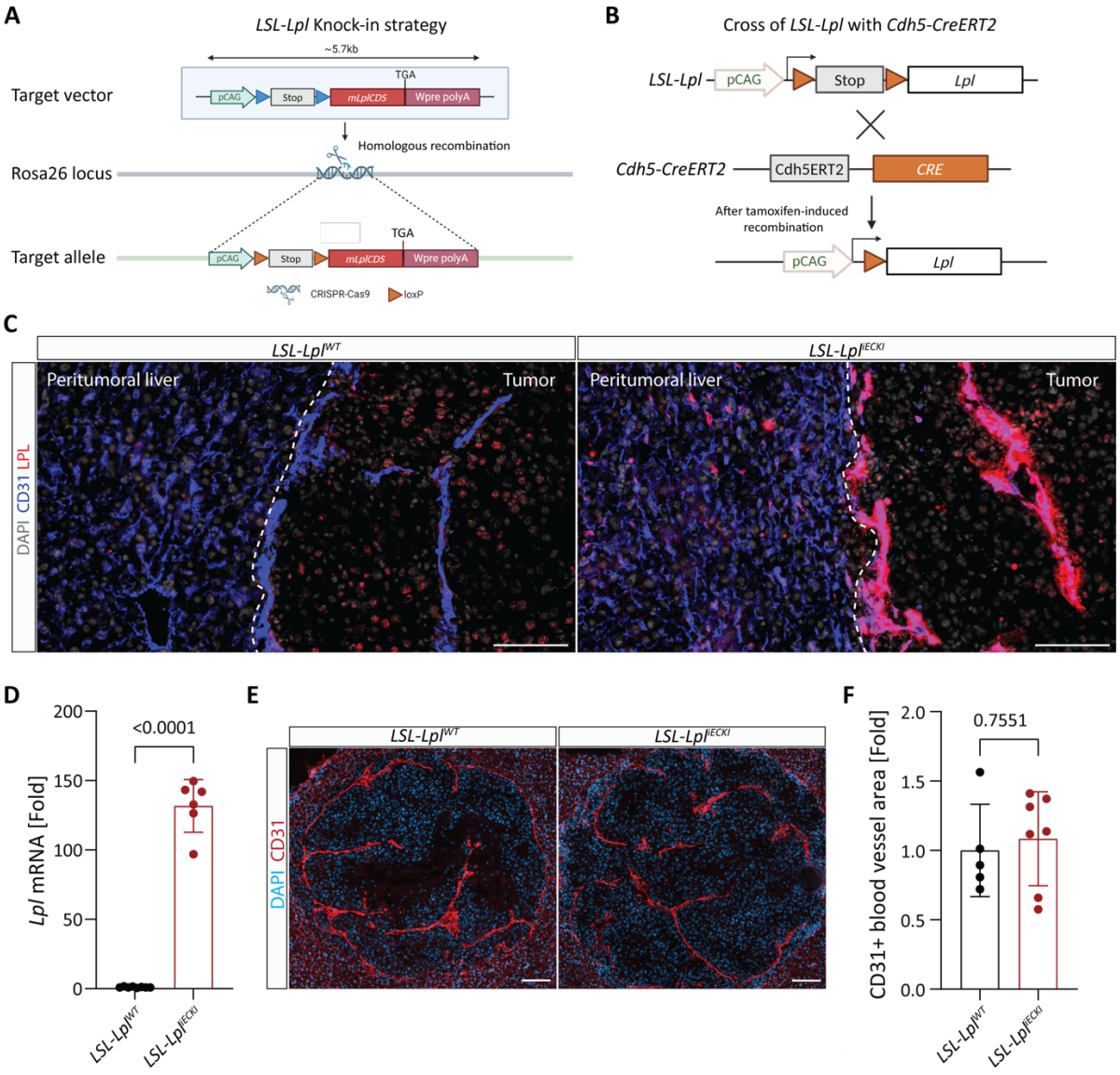

Supplementary Figure S7. Genetic overexpression of *Lpl* in ECs and its influence on intratumoral vessels.

(A) Schematic strategy for the generation of *LSL-Lpl* knock-in allele by homologous recombination via CRISPR/Cas9 system.

(B) Schematic diagram of tamoxifen-induced overexpression of *Lpl* in ECs by crossing *LSL-Lpl* with *Cdh5-CreERT2* mice.

(C) Representative stained images of LPL on OVA-B16F10 metastatic tumor-bearing livers from *LSL-Lpl*^{WT} and *LSL-Lpl*^{iECKI} mice. Scale bar: 100 µm.

(D) QPCR quantitation of *Lpl* expression in liver ECs isolated from tamoxifen-treated *LSL-Lpl*^{WT} and *LSL-Lpl*^{iECKI} mice. N = 6-8 mice per group. Data are presented as mean ± s.d., normalized to *LSL-Lpl*^{WT} samples. Two-tailed Mann-Whitney U test.

(E) Representative images of CD31 stained liver OVA-B16F10 metastatic tumors. Scale bar: 100 µm.

(F) Quantitation of intratumoral blood vessel area in liver metastatic tumors from tamoxifen-treated *LSL-Lpl*^{WT} and *LSL-Lpl*^{iECKI} mice. N = 5-7 mice per group. Data are presented as mean ± s.d., normalized to *LSL-Lpl*^{WT} samples. Two-tailed Mann-Whitney U test.

Supplementary Figure S8

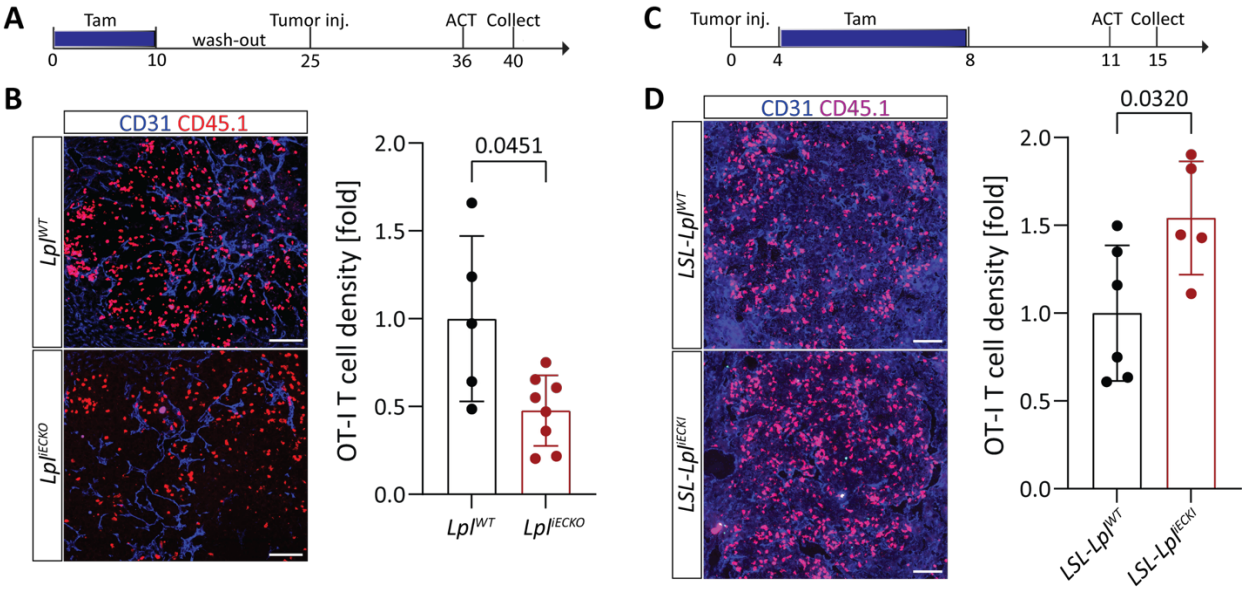

Supplementary Figure S8. Effect of endothelial LPL on OT-I T cell infiltration in the OVA-LLC liver metastatic model.

(A) Experimental design. Mice were first treated with tamoxifen to induce *Lpl* deletion in ECs. After a wash-out period, OVA-LLC cells were intrasplenically injected to induce liver metastases. 11 days after tumor cell injection, mice received ACT of CD8+ OT-I T cells intravenously. Livers were collected 4 days after ACT.

(B) Left, representative images showing intratumoral OT-I T cells in liver metastatic OVA-LLC tumors after ACT. Right, quantitation of infiltrated OT-I T cells. N = 5-8 mice per group. Data are presented as mean ± s.d., normalized to Lpl^{WT} samples. Two-tailed Mann-Whitney U test. Scale bar: 100 μm.

(C) Experimental design. OVA-LLC cells were intrasplenically injected to induce liver metastases. Mice were treated with tamoxifen 4 days after tumor cell injection to overexpress *Lpl* in ECs. 11 days after tumor cell injection, mice received ACT of CD8+ OT-I T cells intravenously. Livers were collected 4 days after ACT.

(D) Left, representative images showing intratumoral OT-I T cells in liver metastatic OVA-LLC tumors after ACT. Right, quantitation of infiltrated OT-I T cells. N = 5-6 mice per group. Data are presented as mean ± s.d., normalized to *LSL-*Lpl^{WT} samples. Two-tailed Mann-Whitney U test. Scale bar: 100 μm.

Supplementary Figure S9

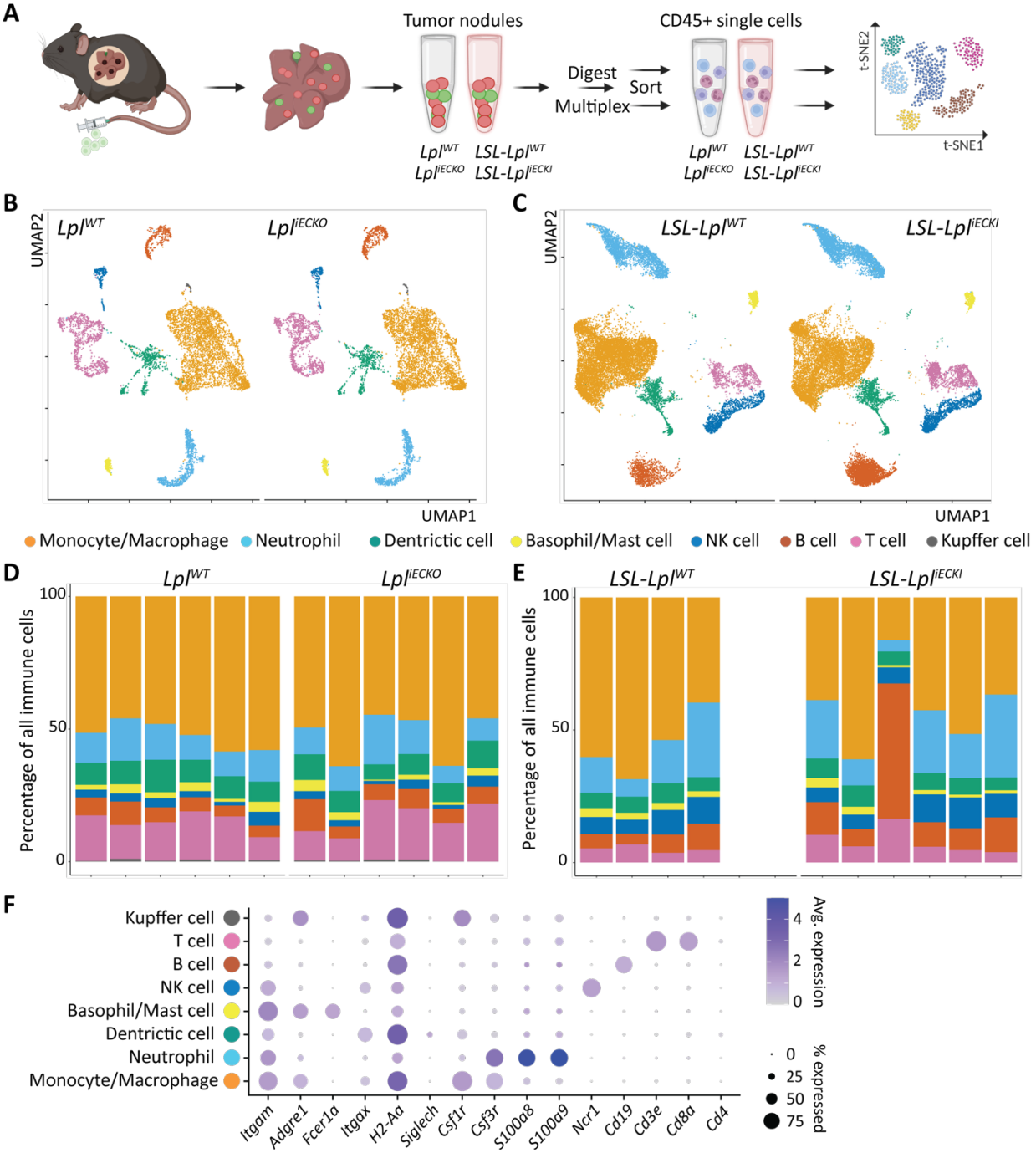

Supplementary Figure S9. Single-cell characterization of the immune landscape of liver metastatic tumors with endothelial LPL intervention.

(A) Experimental strategy of single-cell analysis of tumor-infiltrated immune cells isolated from macrodissected OVA-B16F10 liver metastatic tumors from *Lpl*^{WT}, *Lpl*^{iECKO} as well as *LSL-Lpl*^{WT} and *LSL-Lpl*^{iECKI} mice.

(B) UMAP overview of different immune cell populations retrieved from *Lpl*^{WT} and *Lpl*^{iECKO} mice at the Early time point after ACT.

(C) UMAP overview of different immune cell populations from *LSL-Lpl*^{WT} and *LSL-Lpl*^{iECKI} mice at the Early time point after ACT.

(D) Barchart showing the composition of different tumor-infiltrated immune cell populations in each biological replicate from *Lpl*^{WT} and *Lpl*^{iECKO} mice at the Early time point after ACT. N = 6 mice per group.

(E) Barchart showing the composition of different tumor-infiltrated immune cell populations in each biological replicate isolated from *LSL-Lpl*^{WT} and *LSL-Lpl*^{iECKI} mice at the Early time point after ACT. N = 4-6 mice per group.

(F) Dotplot of marker genes for each immune cell cluster.

Supplementary Figure S10

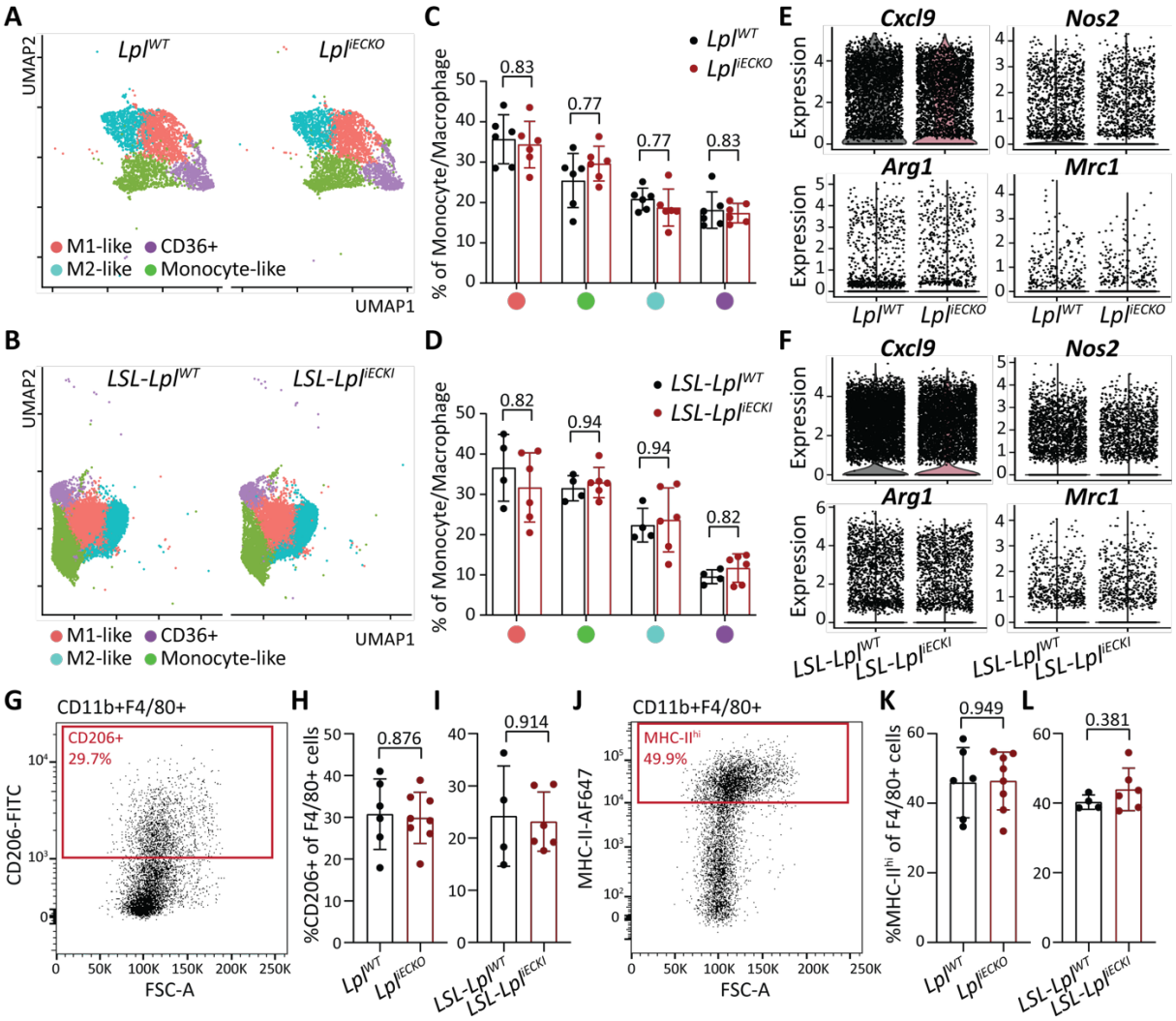

Supplementary Figure S10. Characterization of tumor-associated monocytes/macrophages with EC-LPL intervention.

(A,B) UMAP overview of different macrophage clusters retrieved from *Lpl*^{WT} and *Lpl*^{iECKO} **(A)** as well as *LSL-Lpl*^{WT} and *LSL-Lpl*^{iECKI} **(B)** mice at the Early time point after ACT.

(C,D) Quantitation of different macrophage clusters retrieved from *Lpl*^{WT} and *Lpl*^{iECKO} **(C)** as well as *LSL-Lpl*^{WT} and *LSL-Lpl*^{iECKI} **(D)** mice at the Early time point after ACT. N = 4-6 mice per group. Multiple Mann-Whitney test.

(E,F) Violin plot showing the expression of M1/M2 marker genes in macrophages from *Lpl*^{WT} and *Lpl*^{iECKO} **(E)** as well as *LSL-Lpl*^{WT} and *LSL-Lpl*^{iECKI} **(F)** mice at the Early time point after ACT.

(G) Cytometric analysis of CD206+ population in CD11b+F4/80+ immune cells.

(H-I) Quantitation of CD206+ population in CD11b+F4/80+ immune cells from *Lpl*^{WT} vs *Lpl*^{iECKO} **(H)** and *LSL-Lpl*^{WT} vs *LSL-Lpl*^{iECKI} **(I)** mice at the Early time point after ACT. N = 6-8 mice (*Lpl*^{iECKO}) and 4-6 mice (*LSL-Lpl*^{iECKI}) per group. Two-tailed Mann-Whitney U test.

(J) Cytometric analysis of MHC-II surface abundance in CD11b+F4/80+ immune cells.

(K-L) Quantitation of MHCII^{hi} population in CD11b+F4/80+ immune cells from *Lpl*^{WT} vs *Lpl*^{iECKO} **(K)** and *LSL-Lpl*^{WT} vs *LSL-Lpl*^{iECKI} **(L)** mice at the Early time point after ACT. N = 6-8 mice (*Lpl*^{iECKO}) and 4-6 mice (*LSL-Lpl*^{iECKI}) per group. Two-tailed Mann-Whitney U test.

Supplementary Figure S11

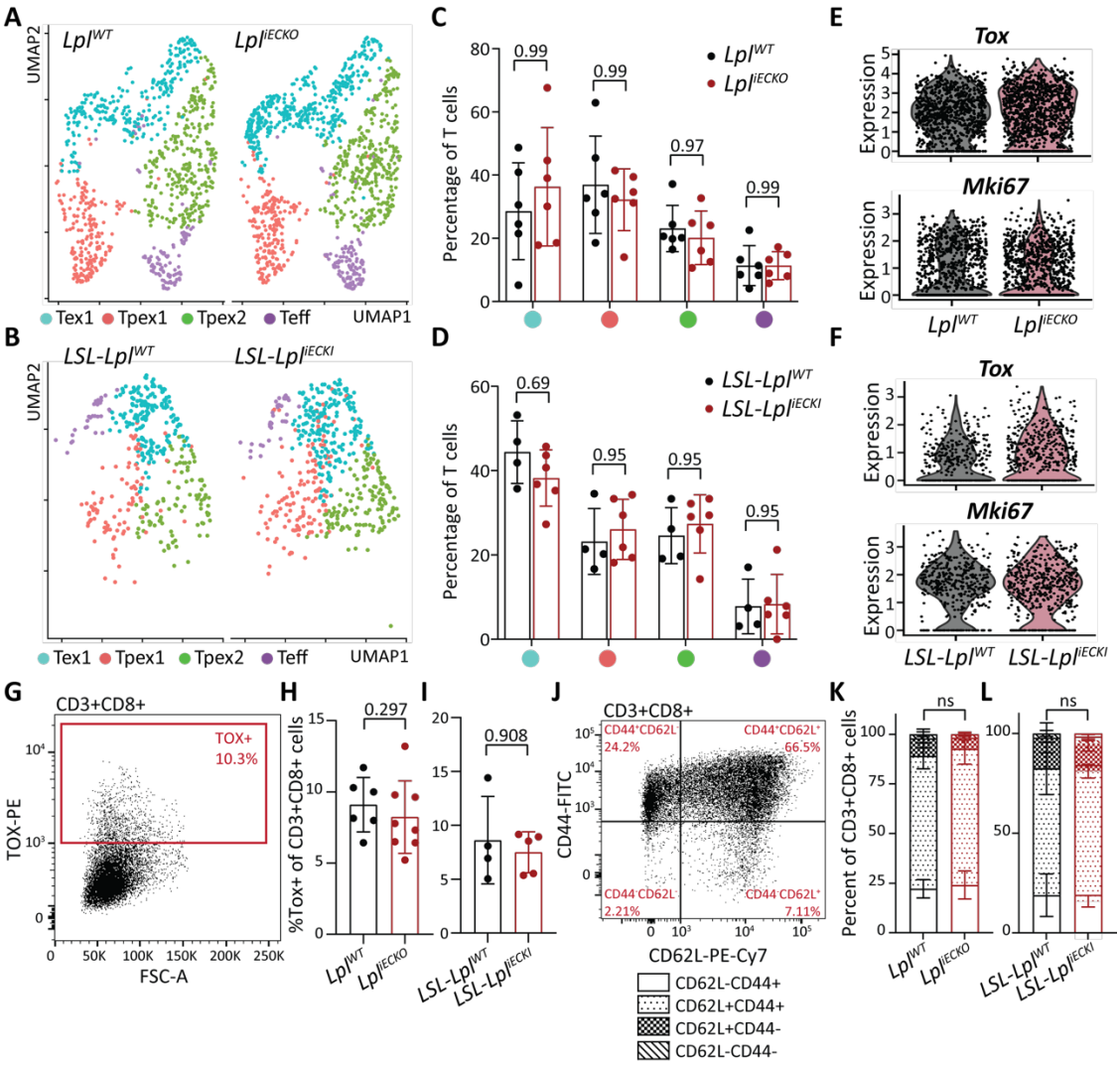

Supplementary Figure S11. Characterization of intratumoral CD8+ T cells with EC-LPL intervention.

(A,B) UMAP overview of different CD8+ T cell clusters retrieved from *Lpl*^{WT} and *Lpl*^{iECKO} **(A)** as well as *LSL-Lpl*^{WT} and *LSL-Lpl*^{iECKI} **(B)** mice at the Early time point after ACT.

(C,D) Quantitation of different CD8+ T cell clusters retrieved from *Lpl*^{WT} and *Lpl*^{iECKO} **(C)** as well as *LSL-Lpl*^{WT} and *LSL-Lpl*^{iECKI} **(D)** mice at the Early time point after ACT. N = 4-6 mice per group. Multiple Mann-Whitney test.

(E,F) Violin plot showing *Tox* and *Mki67* expression in CD8+ T cells from *Lpl*^{WT} and *Lpl*^{iECKO} **(E)** as well as *LSL-Lpl*^{WT} and *LSL-Lpl*^{iECKI} **(F)** mice at the Early timepoint after ACT.

(G) Cytometric analysis of TOX+ population in CD3+CD8+ T cells.

(H-I) Quantitation of TOX+ population in CD3+CD8+ T cells from *Lpl*^{WT} vs *Lpl*^{iECKO} **(H)** and *LSL-Lpl*^{WT} vs *LSL-Lpl*^{iECKI} **(I)** mice at the Late time point after ACT. N = 6-8 mice (*Lpl*^{iECKO}) and 4-5 mice (*LSL-Lpl*^{iECKI}) per group. Two-tailed Mann-Whitney U test.

(J) Cytometric analysis of CD44 amd CD62L surface abundance in CD3+CD8+ T cells.

(K-L) Quantitation of different status (based on CD44 and CD62L abundance) of CD3+CD8+ T cells from *Lpl*^{WT} vs *Lpl*^{iECKO} **(K)** and *LSL-Lpl*^{WT} vs *LSL-Lpl*^{iECKI} **(L)** mice at the Late time point after ACT. N = 6-8 mice (*Lpl*^{iECKO}) and 4-5 mice (*LSL-Lpl*^{iECKI}) per group. Two-way ANOVA test.

Supplementary Figure S12

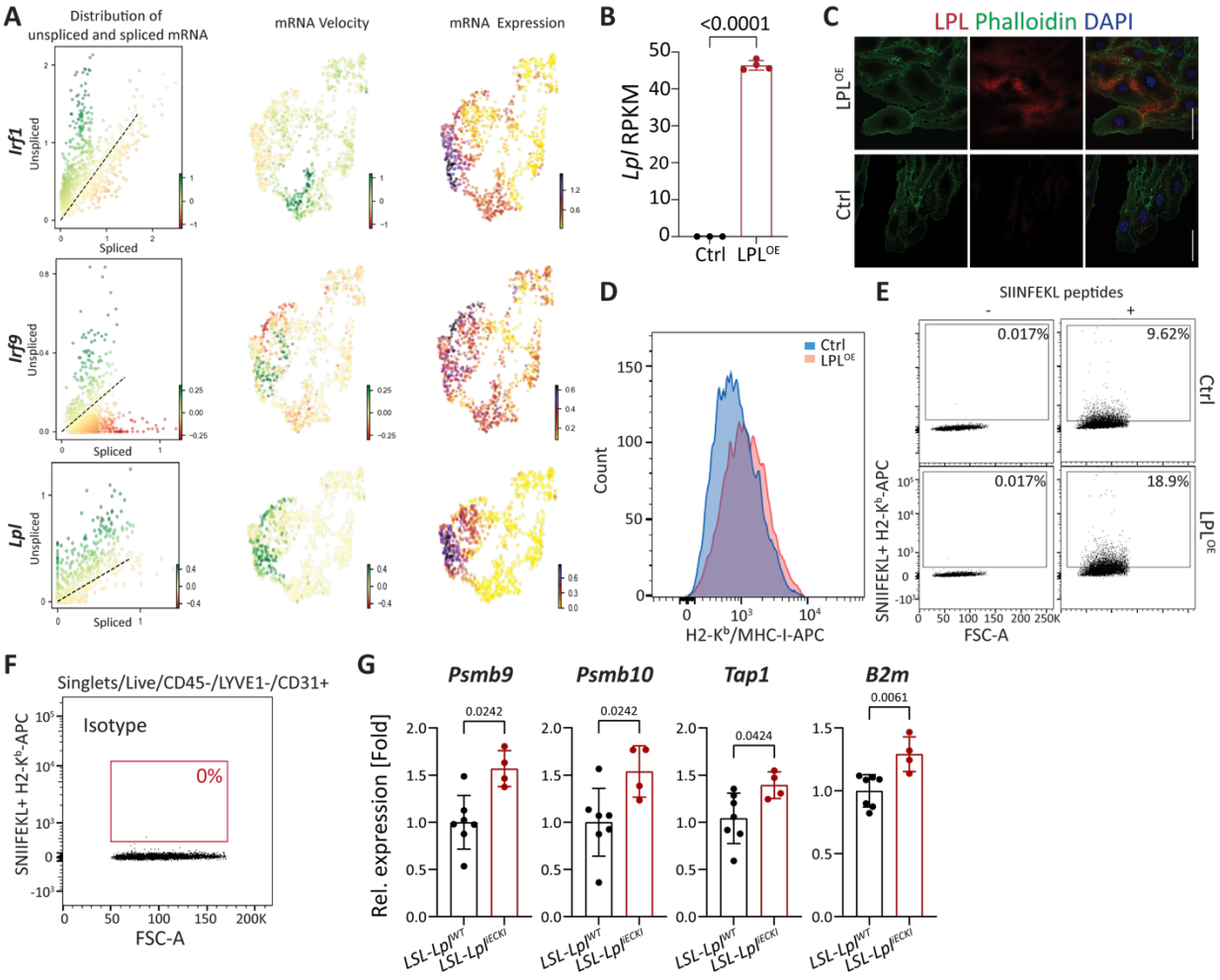

Supplementary Figure S12. Endothelial LPL upregulation results in the activation of molecules related to MHC-I-mediated antigen presentation.

(A) Messenger RNA expression and velocity of *Irf1*, *Irf9,* and *Lpl* across Ctrl- and Early- TECs from scRNAseq data.

(B) Dot plot showing *Lpl* expression in bulk RNA sequencing data from Ctrl- and *Lpl*-overexpressing ECs. N = 4 replicates per group. Data are presented as mean ± s.d. Two-tailed student's T test.

(C) Representative stained images of *in vitro* cultured Ctrl- and *Lpl*-overexpressing ECs. Scale bar: 5 μm.

(D) Histogram of H2-K^b/MHC-I surface abundance on *in vitro* cultured Ctrl- and *Lpl*-overexpressing ECs.

(E) Cytometric analysis of SIINFEKL-H2-K^b surface presentation by *in vitro* cultured Ctrl- and *Lpl*-overexpressing ECs.

(F) Cytometric analysis of Isotype control on TECs isolated from primary OVA-B16F10 tumors challenged with activated OT-I T cells or control PBS for 48 hours (corresponding to Fig. 4G).

(G) Gene expression of *Psmb9*, *Psmb10, Tap1,* and *B2m* in TECs isolated from OVA-B16F10 primary tumors grown in *LSL-Lpl^{WT}* and *LSL-Lpl^{iECKI}* mice. N = 4-7 replicates per group. Data are presented as mean ± s.d., normalized to *LSL-Lpl^{WT}* samples. Two-tailed Mann-Whitney U test.

Supplementary Figure S13

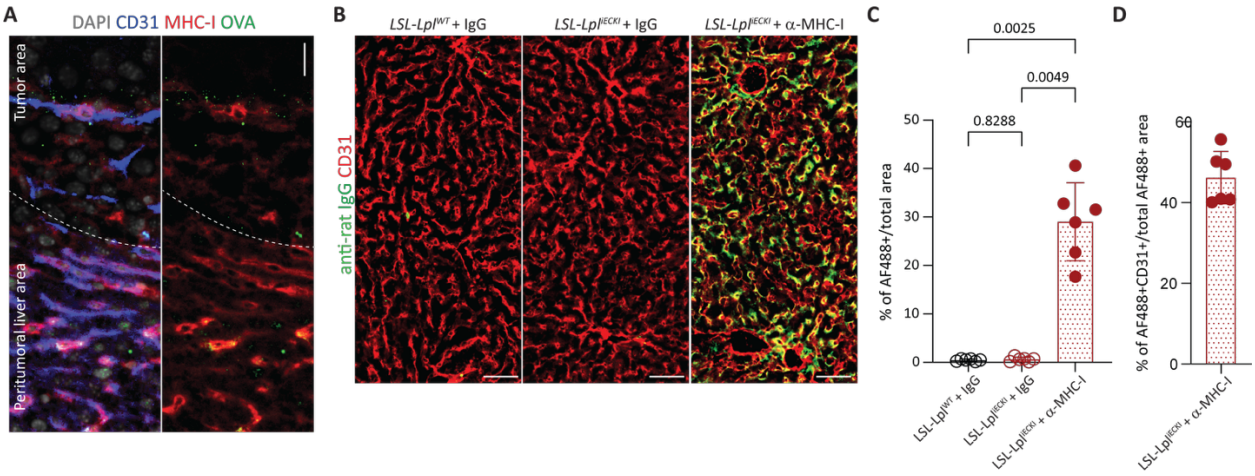

Supplementary Figure S13. *In vivo* MHC-I blocking experiment.

(A) Representative staining of H2-K^b/MHC-I on liver metastatic OVA-B16F10 tumor nodules. Scale bar: 20 μm.

(B) Representative images of CD31 and anti-rat IgG (representing MHC-I blocking antibody) in peritumoral liver area. Scale bar: 50 μm.

(C) Quantitation of the percentage of αMHC-I bound area (AF488+ area) in peritumoral liver tissue specimens. N = 6 livers per group. Data are presented as mean ± s.d. One-way ANOVA test.

(D) Quantitation of αMHC-I bound CD31+ vascular area (AF488+CD31+) to total AF488+ area in peritumoral liver area of αMHC-I-treated *LSL-LPL^{iECKI}* group . N = 6 livers per group. Data are presented as mean ± s.d.

Supplementary Figure S14

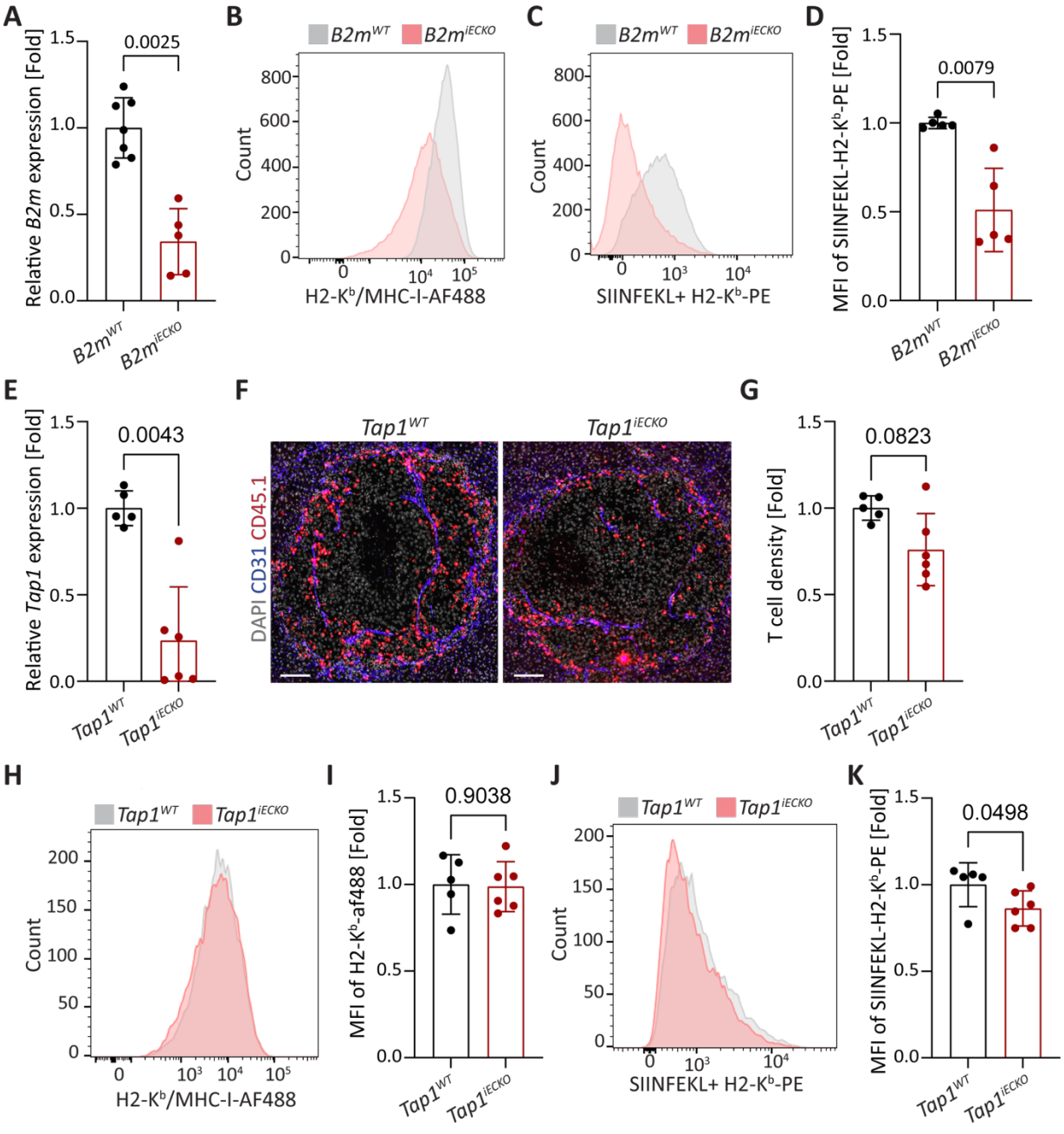

Supplementary Figure S14. Endothelial antigen presentation facilitates T cell infiltration into liver metastatic tumors.

(A) QPCR quantitation of *B2m* expression in liver ECs from tamoxifen-treated *B2m*^{WT} and *B2m*^{iECKO} mice. N = 5-7 mice per group. Data are presented as mean ± s.d., normalized to *B2m*^{WT} samples. Two-tailed Mann-Whitney U test.

(B) Cytometric analysis of H2-K^b/MHC-I presentation on the cell surface of ECs isolated from metastasis-bearing livers of tamoxifen-treated *B2m*^{WT} and *B2m*^{iECKO} mice.

(C,D) Cytometric analysis **(C)** and quantitation **(D)** of OVA peptide SIINFEKL loaded-H2-K^b on the cell surface of ECs isolated from metastasis-bearing livers of tamoxifen-treated $B2m^{WT}$ and $B2m^{iECKO}$ mice. N = 5 mice per group. Data are presented as mean ± s.d. Two-tailed Mann-Whitney U test.

(E) QPCR quantitation of *Tap1* expression in liver ECs from tamoxifen-treated $Tap1^{WT}$ and $Tap1^{iECKO}$ mice. N = 5-6 mice per group. Data are presented as mean ± s.d., normalized to $Tap1^{WT}$ samples. Two-tailed Mann-Whitney U test.

(F,G) Representative images **(F)** and quantitation **(G)** of intratumoral OT-I T cells in OVA-B16F10 liver metastatic tumors from tamoxifen-treated $Tap1^{WT}$ and $Tap1^{iECKO}$ mice. N = 5-6 livers per group. Data are presented as mean ± s.d., normalized to $Tap1^{WT}$ samples. Two-tailed Mann-Whitney U test. Scale bar: 200 μm.

(H, I) Cytometric analysis **(H)** and quantitation **(I)** of H2-K^b/MHC-I presentation on the cell surface of ECs isolated from metastasis-bearing livers of tamoxifen-treated $Tap1^{WT}$ and $Tap1^{iECKO}$ mice. N = 5-6 livers per group. Data are presented as mean ± s.d., normalized to $Tap1^{WT}$ samples. Two-tailed Mann-Whitney U test.

(J,K) Cytometric analysis **(J)** and quantitation **(K)** of OVA peptide SIINFEKL loaded-H2-K^b on the cell surface of ECs isolated from metastasis-bearing livers of tamoxifen-treated $Tap1^{WT}$ and $Tap1^{iECKO}$ mice. N = 5-6 mice per group. Data are presented as mean ± s.d., normalized to $Tap1^{WT}$ samples. Two-tailed Mann-Whitney U test.

Supplementary Figure S15

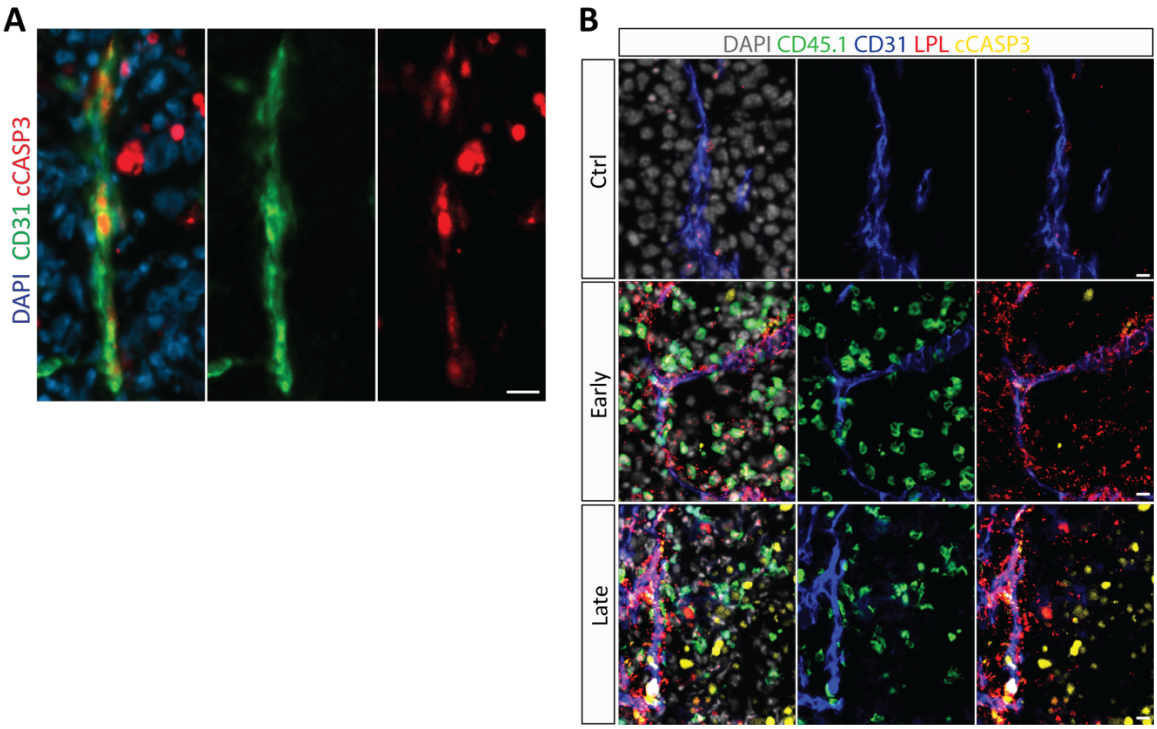

Supplementary Figure S15. Analysis of EC death after ACT of activated OT-I T cells.

(A) Representative staining of cleaved-Caspase3 (cCASP3) in OVA-B16F10 liver metastatic tumor nodules collected 4 days after ACT. Scale bar: 10 μm.

(B) Representative stained images of CD45.1, CD31, cCASP3, and LPL in OVA-B16F10 liver metastatic tumors collected at Ctrl, Early and Late timepoints after ACT. Scale bar: 10 μm.

Supplementary Figure S16

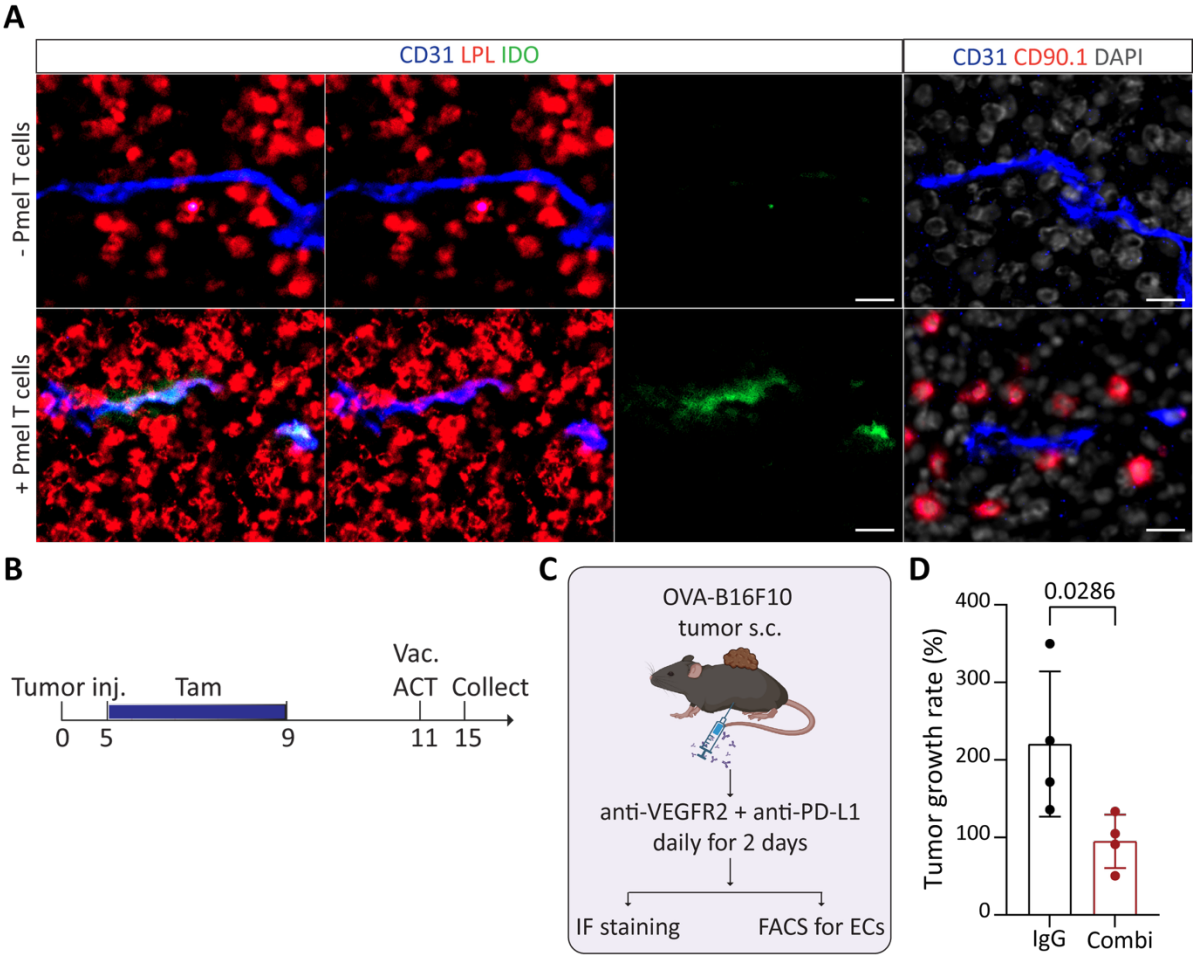

Supplementary Figure S16. Assessment of LPL+ TECs in clinically-relevant intervention models.

(A) Representative images of CD31, CD90.1 (Pmel T cells), LPL, IDO, and DAPI stainings on Hcmel12 liver metastatic tumors nodules collected at 4 days after ACT of Pmel T cells. Scale bar: 20 μm.

(B) Experimental design. B16F10 cells were intrasplenically injected to initiate liver metastases. Mice were treated with tamoxifen 5 days after tumor cell inoculation to overexpress *Lpl* in ECs. At 11 days after tumor cell injection, 10μg hgp100 peptide was injected intraperitoneally for vaccination and ACT of Pmel T cells was performed 6h later into mice. Livers were collected 4 days after ACT.

(C) Experimental design for evaluating LPL levels in tumor ECs in mice treated with a combination of anti-VEGFR2 and anti-PD-L1 therapy.

(D) Quantification of tumor growth rate in mice 3 days after treatment with a combination of anti-VEGFR2 and anti-PD-L1 therapy or control IgG. N = 4 per group. Data are presented as mean ± s.d. Two-tailed Mann-Whitney U test.

Supplementary Figure S17

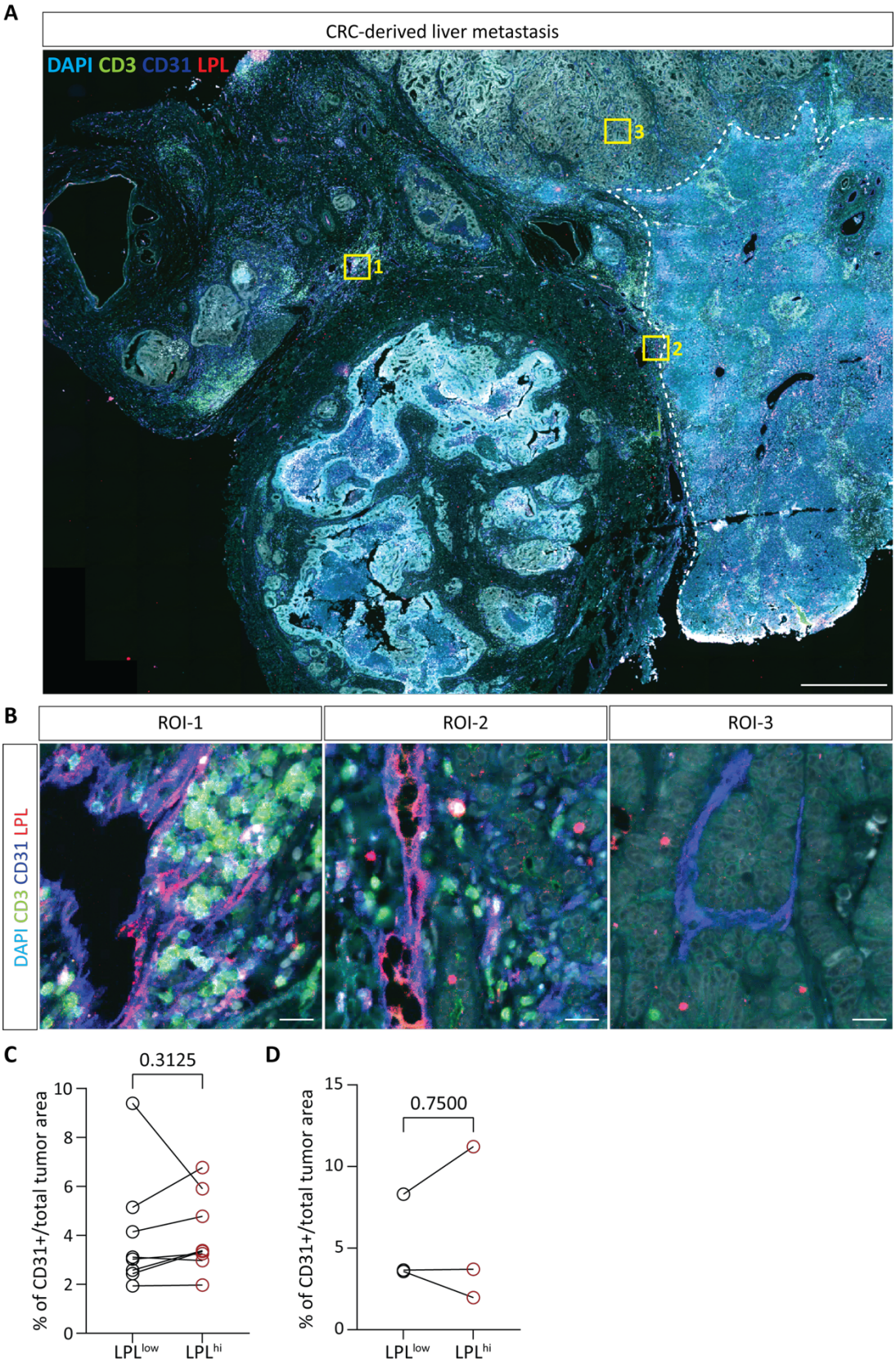

Supplementary Figure S17. Staining of LPL on human CRC-derived liver metastatic tumor tissue.

(A) Overview image of human colorectal cancer-derived liver metastatic tissue stained with DAPI, CD3, CD31, and LPL. Scale bar: 1 mm.

(B) Zoomed-in images of regions of interest (ROI) from (a). Scale bar: 20 μm.

(C) Quantitation of CD31+ blood vessel area in the analyzed tumor area with either LPL^{low} or LPL^{hi} blood vessels in human CRC-derived liver metastatic tumors. N = 8 human tumors. Data are presented as matched pairs. Paired T test.

(D) Quantitation of CD31+ blood vessel area in the analyzed tumor area with either LPL^{low} or LPL^{hi} blood vessels in human melanoma-derived liver metastatic tumors. N = 3 human tumors. Data are presented as matched pairs. Paired T test.